Solid Earth Discuss., 7, 3817–3841, 2015
www.solid-earth-discuss.net/7/3817/2015/
doi:10.5194/sed-7-3817-2015
© Author(s) 2015. CC Attribution 3.0 License.

Solid Earth
Discussions
Open Access

This discussion paper is/has been under review for the journal Solid Earth (SE).
Please refer to the corresponding final paper in SE if available.

A simple 3-D numerical model of thermal convection in Earth's growing inner core: on the possibility of the formation of the degree-one structure with lateral viscosity variations

M. Yoshida

Department of Deep Earth Structure and Dynamics Research, Japan Agency for Marine-Earth Science and Technology (JAMSTEC), 2–15 Natsushima-cho, Yokosuka, Kanagawa 237-0061, Japan

Received: 4 December 2015 – Accepted: 6 December 2015 – Published: 15 December 2015

Correspondence to: M. Yoshida (myoshida@jamstec.go.jp)

Published by Copernicus Publications on behalf of the European Geosciences Union.

Abstract

An east-west hemispherically asymmetric structure for Earth's inner core has been suggested by various seismological evidence, but its origin is not clearly understood. Here, to investigate the possibility of an "endogenic origin" for the degree-one thermal/mechanical structure of the inner core, I performed new numerical simulations of thermal convection in the growing inner core. A setup value that controls the viscosity contrast between the inner core boundary and the interior of the inner core, $\Delta\eta_T$, was taken as a free parameter. Results show that the degree-one structure only appeared for a limited range of $\Delta\eta_T$; such a scenario may be possible but is not considered probable for the real Earth. The degree-one structure may have been realized by an "exogenous factor" due to the planetary-scale thermal coupling among the lower mantle, the outer core, and the inner core, not by an endogenic factor due to the internal rheological heterogeneity.

1 Introduction

After the segregation of the rocky mantle and molten iron core in the early stage of Earth's formation (e.g., Stevenson, 1981), the inner core was formed by gradual solidification of the molten iron core and the size increased with age (Jacobs, 1953; Buffett et al., 1992) (for example, see reviews by Buffett, 2000 and Sumita and Yoshida, 2003). The solidification of the solid core could affect the vigor of outer-core convection owing to the release of latent heat and the passage of light elements toward the liquid outer core (e.g., Sumita and Yoshida, 2003). The resulting growth of the inner core may have changed the convection style in the outer core and affected the intensity of Earth's magnetic field throughout Earth's history.

Although the structure of the present inner core cannot be inferred from surface geophysical observations, various seismological evidence suggests that the inner core has an east-west, hemispherically asymmetric structure in terms of seismic velocity,

CC BY

anisotropy, and attenuation (Tanaka and Hamaguchi, 1997; Creager, 1999; Niu and Wen, 2001; Cao and Romanowicz, 2004; Deuss et al., 2010; Irving and Deuss, 2011; Waszek et al., 2011; Lythgoe et al., 2014) (see also a recent review by Tkalčić, 2015).

Previous numerical simulations of Earth's mantle convection clarified that for convecting rocky materials confined in a spherical shell, the spherical harmonic degree-one structure was observed for a relatively wide range of the parameter that controls the lateral viscosity variations due to temperature variations (McNamara and Zhong, 2005; Yoshida and Kageyama, 2006). This is because when the temperature-dependence of viscosity is moderate, the highly viscous lid that develops at the surface of the convecting mantle has the longest-wavelength scale, and the dynamic instability at the bottom of the lid concentrates in one area. This scenario characterizes the degree-one thermal structure of mantle convection that lies between the "mobile-lid regime" with weakly temperature-dependent viscosity and the "stagnant-lid regime" with strongly temperature-dependent viscosity (Yoshida and Kageyama, 2006).

It is possible that the degree-one seismic structure in the present inner core originated from lateral temperature variations, which in turn originated from lateral viscosity variations. Even given the uncertainties in the rheological properties and composition of the inner core materials, lateral viscosity variation offers considerable potential as an "endogenic factor" that may explain the formation of the degree-one seismic structure. It is therefore worth examining whether a degree-one thermal/mechanical structure generated from the lateral viscosity variations can be realized for solid materials confined in a sphere. This topic had not been investigated in previous numerical simulation models of inner core convection (Deguen and Cardin, 2011; Cottaar and Buffett, 2012; Deguen, 2013; Deguen et al., 2013).

In this study, to explore the time-dependent behavior of the convection regime in Earth's growing inner core and the possibility of generating the degree-one thermal/mechanical structure from the internal rheological heterogeneity, a new simple numerical model of the growing inner core is constructed and a series of numerical simulations of thermal convection are performed, assuming that the solidification of the liquid core started at 4.5 Ga and that the radius of the inner core gradually increased with the square root of age.

2 Model

Convection in the inner core is computed numerically using a staggered grid-based, finite-volume code, ConvGS (e.g., Yoshida, 2008). The material of the inner core is modeled as a Boussinesq fluid with an infinite Prandtl number confined in a sphere and modeled in spherical coordinates (r, θ, φ). Impermeable, shear-stress-free, isothermal conditions are imposed on the inner core boundary (ICB) with a fixed dimensionless radius of $r'_c = 1$ (Fig. 1a). The driving force of convection is primordial heat alone because the radiogenic heat production is negligibly small in the inner core (e.g., Karato, 2003). The number of computational grids is taken as $64(r) \times 64(\theta) \times 192(\varphi) \times 2$ (for Yin and Yang grids) (Yoshida and Kageyama, 2004). To avoid the mathematical singularity at the Earth's center, an extremely small sphere with a dimensionless radius of $r'_\delta = 10^{-6}$ is imposed at the center of the model sphere.

Following standard techniques for mantle convection simulations (e.g., Schubert et al., 2001), the length L, velocity vector $\boldsymbol{v}$, stress tensor (or pressure) σ, viscosity η, time t, and temperature T are non-dimensionalized as follows:

$$L = r_c(t)L', \boldsymbol{v} = \frac{\kappa_0}{r_c(t)}\boldsymbol{v}', \sigma = \frac{\kappa_0 \eta_0}{r_c(t)^2}\sigma', \eta = \eta_0 \eta', t = \frac{r_c(t)^2}{\kappa_0}t', T = \Delta T_0 \cdot T' \quad (1)$$

where $r_c(t)$ denotes the time-dependence of the radius of the inner core, which depends on time (age); κ_0 denotes the reference thermal diffusivity; η_0, the reference viscosity; ΔT_0, the reference temperature difference; and the subscript "0" refers the reference values for the inner core (Table 1). In these equations, symbols with primes represent dimensionless quantities.

Discussion Paper | Discussion Paper | Discussion Paper | Discussion Paper |

SED

7, 3817–3841, 2015

A simple 3-D numerical model of thermal convection in Earth's growing inner core

M. Yoshida

CC BY

Using these dimensionless factors, the dimensionless conservation equations for mass, momentum, and energy, which govern inner core convection, are expressed as

$$\nabla \cdot \boldsymbol{v} = 0, \tag{2}$$

$$-\nabla p + \nabla \cdot \tau + \mathrm{Ra}(t)\zeta(t)^{-3} T \boldsymbol{e}_\mathrm{r} = 0, \tau = \eta \left(\nabla \boldsymbol{v} + \nabla \boldsymbol{v}^{tr}\right) \tag{3}$$

$$\frac{\partial T}{\partial t} + \boldsymbol{v} \cdot \nabla T = \nabla^2 T + H(t)\zeta(t)^{-2}, \tag{4}$$

respectively, where p represents the pressure; τ, the deviatoric stress tensor; and $\boldsymbol{e}_\mathrm{r}$, the unit vector in the radial direction. Primes representing dimensionless quantities are omitted in Eq. (2–4).

In the numerical simulation for this study, instead of fixing the dimensionless radius of the ICB, the radius of the inner core in the thermal Rayleigh number, Ra, the internal heat-source number, H, and the “spherical-shell ratio”, ζ, depend on age. They are given by

$$\mathrm{Ra}(t) \equiv \frac{\rho_0^2 \alpha_0 \Delta T_0 g_0 c_{\mathrm{p}0} \left[r_\mathrm{c}(t) - r_\delta\right]^3}{k_0 \eta_0}, H(t) \equiv \frac{\Omega \rho_0 \left[r_\mathrm{c}(t) - r_\delta\right]^2}{M_\mathrm{m} \Delta T_0 k_0}, \zeta(t) \equiv \frac{r_\mathrm{c}(t) - r_\delta}{r_\mathrm{c}(t)}, \tag{5}$$

where ρ_0 is the reference density; α_0, the reference thermal expansion coefficient; ΔT_0, the reference temperature difference across the inner core; g, the reference gravitational acceleration; $c_{\mathrm{p}0}$, the reference specific heat at constant pressure; k_0, the reference thermal conductivity; and M_m, the mass of the mantle (Table 1). Thermal conductivity has received a lot of attention in recent mineral physics studies, and the main finding is that it may be much larger than the value of $36\,\mathrm{W\,m^{-1}\,K^{-1}}$ from Stacey and Davis (2008), i.e., 100–$200\,\mathrm{W\,m^{-1}\,K^{-1}}$ (de Koker et al., 2012; Pozzo et al., 2012, 2014). Therefore, two end-member models with $k_0 = 36$ and $200\,\mathrm{W\,m^{-1}\,K^{-1}}$ are investigated in this study.

The amount of approximated primordial heat that has existed since Earth’s formation, Ω, is taken as a free parameter estimated from the heat released by mantle cooling in

SED
7, 3817–3841, 2015

CC BY

the present Earth (Turcotte and Schubert, 2014):

$$\Omega = -\frac{4}{3}\pi r_e^3 \rho_e c_{pe0} \left.\frac{dT}{dt}\right|_{t=t_0}, \tag{6}$$

where r_e is the radius of Earth; ρ_e, the average density of Earth; and c_{pe0}, the average specific heat at constant pressure for Earth. Here $dT/dt\,|_{t=t_0}$ is the present cooling rate of the mantle (Turcotte and Schubert, 2014):

$$\left.\frac{dT}{dt}\right|_{t=t_0} = -3\lambda\left(\frac{RT_m^2}{E_a}\right), \tag{7}$$

where λ is the average radiogenic decay constant in the mantle; R, the gas constant, T_m, the mean mantle temperature; and E_a, the activation energy of dry olivine. Using the values in Table 1, Ω is 11.3 TW, which is a reasonable value compared with the total heat release by mantle cooling estimated from a global heat-flow balance (Lay et al., 2008).

Following the work of Buffett et al. (1992), who studied an analytical model for solidification of the inner core, the global heat balance of the outer core is

$$\frac{4\pi}{3}\left(r_b^3 - r_c^3\right)\rho c_p \frac{dT_s(r)}{dt} = 4\pi r_c^2 f_i(t) - 4\pi r_b^2 f_m(t), \tag{8}$$

where $T_s(r)$ is the "solidification temperature", and $f_i(t)(\equiv F_i(t)/(4\pi r_c^2))$ and $f_m(t)(\equiv F_m(t)/(4\pi r_b^2))$ are the heat fluxes across the ICB and the core-mantle boundary (CMB), respectively (Fig. 1b). The potential temperature in the well-mixed liquid outer core is assumed to be spatially uniform and slowly decreases with time, and the ICB is assumed to be in thermodynamic equilibrium with the surrounding liquid. Under these assumptions, the temperature through the outer core is uniquely defined by the solidification temperature, $T_s(r)$, as a function of pressure or depth (see the explanation

Discussion Paper | Discussion Paper | Discussion Paper | Discussion Paper |

SED

7, 3817–3841, 2015

A simple 3-D numerical model of thermal convection in Earth's growing inner core

M. Yoshida

CC BY

in Buffett et al., 1992 for details). Here, the heat sources associated with solidification of the inner core (i.e., the release of latent heat and gravitational energy) are ignored because these effects play a secondary role in the growth of the inner core (Buffett et al., 1992).

According to Eq. (4) in Buffett et al. (1992), the radial dependence of T_s is expressed as

$$T_s(r) = T_s(0) - \frac{2\pi}{3} G \rho_0^2 r^2 \frac{\partial T_s}{\partial p}, \tag{9}$$

where G is the gravitational constant, and $\partial T_s / \partial p$ is the solidification profile (Table 1).

Substituting Eq. (9) into Eq. (8), an expression for the radius of the inner core is obtained:

$$r_c(t) = r_b \left[\frac{1}{4\pi r_b^2 N} \int_0^t F_m(t) dt \right]^{\frac{1}{2}}, \tag{10}$$

where the model constant N is expressed as

$$N = \frac{2\pi}{9} r_b^3 c_{p0} \rho_0^2 G \frac{\partial T_s}{\partial p}. \tag{11}$$

Assuming that the heat flux across the CMB is constant throughout Earth's history (Buffett et al., 1992), a model constant, F'_m, is obtained:

$$F'_m = \frac{4\pi N}{t} \left(r_c - r_c^i \right)^2, \tag{12}$$

where r_c^i is an arbitrary value that represents the initial radius of the inner core at the beginning of the simulation. When the age of Earth's core is assumed to be 4.5 Ga (Lister and Buffett, 1998), the solidification of the inner core is assumed to have begun

SED
7, 3817–3841, 2015

cc BY

at this age, and r_c^i is taken to be 21.5 km so that $r_c - r_c^i$ is exactly 1200 km, F_m' is 2.56×10^{12} W, which would be a lower limit value for the real Earth considering an even relationship between the total plume buoyancy flux observed at the Earth' surface and the inferred total CMB heat flow (e.g., Davies, 1988; Sleep, 1990; Davies and Richards, 1992). Equation (12) indicates that the relationship between the total CMB heat flow and the radius of the growing inner core is $F_m' \propto r_c^2$, which means that the radius of the inner core is proportional to the square root of F_m'. It should be noted that there is a trade-off between the choices of F_m' and r_c^i, which are critical for identifying the age of the present-day inner core in the real Earth. In the present model, I set r_c^i to a significantly small value to see the behavior of inner core convection over the longest geological time, i.e., 4.5 Gyr (see Sect. 4 for discussion).

Finally, the time-dependent radius of the growing inner core used in the present simulation is expressed as

$$r_c(t) = \left(\frac{F_m'}{4\pi N} \bar{t} \right)^{\frac{1}{2}} + r_c^i, \tag{13}$$

where the dimensional time is scaled as $\bar{t} = (\bar{r}_c(t)^2 / \kappa_0) \cdot t'$ using the radius of the inner core at the previous time step of the simulation, $\bar{r}_c(t)$. Equation (13) means that r_c increases with the square root of age, and eventually reaches $r_c = 1221.5$ km after 4.5 Gyr, which matches the present radius of Earth's inner core.

At the beginning of the simulation, the initial condition for dimensionless temperature with significant small-scale lateral perturbations is given as

$$T'(r,\theta,\phi) = 0.5 + \varpi \cdot Y_{34}^{17}(\theta,\phi) \cdot \sin\left[\pi \frac{r_1' - r'}{r_1'}\right], \tag{14}$$

where $Y_\ell^m(\theta, \phi)$ is the fully normalized spherical harmonic function of degree ℓ and order m and $\varpi(= 0.1)$ is the amplitude of perturbation.

SED
7, 3817–3841, 2015

CC BY

The viscosity of the inner core materials, η'_T, in this model depends on temperature according to a dimensionless formulation (Yoshida, 2014):

$$\eta'_T = \eta'_0 \cdot \exp\left[2T'_{\text{ave}}(t)\left(\frac{E'}{T' + T'_{\text{ave}}(t)} - \frac{E'}{2T'_{\text{ave}}(t)}\right)\right], \quad (15)$$

where $T'_{\text{ave}}(t)$ is the dimensionless average temperature of the entire sphere at each time step. A model parameter, E', controls the viscosity contrast between the ICB with $T' = 0$ and the interior of the inner core. In the present model, $E' = \ln(\Delta\eta_T)$ varies from $\ln(10^0) = 1$ (i.e., no laterally variable viscosity) to $\ln(10^5) = 11.51$.

3 Resutls

Figure 2 shows the time evolution of the convection pattern in the inner core for models with $\eta_0 = 10^{17}$ Pa s, $k_0 = 36\,\text{W m}^{-1}\,\text{K}^{-1}$, and with $\Delta\eta_T = 10^0$ (Fig. 2a–d), $\Delta\eta_T = 10^3$ (Fig. 2e–h), $\Delta\eta_T = 10^{3.5}$ (Fig. 2i–l), and $\Delta\eta_T = 10^4$ (Fig. 2m–p). When $\Delta\eta_T = 10^0$ (i.e., the viscosity of the inner core is homogeneous) the convection pattern kept a short-wavelength structure over almost all of the simulation time and the "present" inner core at 0.0 Ga has numerous downwellings uniformly distributed in the sphere (Fig. 2d). On the other hand, when $\Delta\eta_T$ is large enough to make the surface thermal boundary layer stagnant ($\Delta\eta_T \geq 10^4$), the convection pattern tends towards a short-wavelength structure with age, and secondary cold plumes from the bottom of the highly viscous lid are evenly distributed in the sphere (Fig. 2p). A remarkable change in the convection pattern is found for moderate values of $\Delta\eta_T$: when $\Delta\eta_T = 10^3$ and $10^{3.5}$, the convection patterns shift towards a long-wavelength structure with increasing age, and eventually the longest-wavelength thermal structures develop for the inner core at 0.0 Ga (Fig. 2h and l)

To quantitatively assess the variations in thermal and mechanical heterogeneities in the inner core with time, Fig. 3 shows the power spectra of the temperature and

CC BY

root-mean-square velocity fields throughout the modelled inner core at each time step. On the other hand, when $\Delta\eta_T$ is $\leq 10^{2.5}$, it is found that the scales of the thermal and mechanical heterogeneities generally tend to shorten with increasing age, although long-wavelength structures develop just after the beginning of the simulation ("A" in Fig. 3a and c) in spite of an initial temperature condition with a short-wavelength structure (Eq. 14). When $\Delta\eta_T$ is moderate (i.e., $\Delta\eta_T = 10^3$ and $10^{3.5}$) it appears that the scales of the thermal and mechanical heterogeneities generally tend to shorten with increasing age before c. 2.0 Ga, but the degree-one structure begins to develop after 1.0 Ga (see "B" in Fig. 3e–h).

Even when $\eta_0 = 10^{16}$ Pa s and $k_0 = 36$–$200\ \mathrm{W\,m^{-1}\,K^{-1}}$, these conclusions remain essentially unchanged: the degree-one thermal/mechanical structure only appeared for a limited range of parameter values for lateral viscosity variations, i.e., $\Delta\eta_T = 10^4$ and $10^{4.5}$ for the model with $k_0 = 36\ \mathrm{W\,m^{-1}\,K^{-1}}$ ("A" in Fig. 4) and $\Delta\eta_T = 10^3$ and $10^{3.5}$ for the model with $k_0 = 200\ \mathrm{W\,m^{-1}\,K^{-1}}$ ("A" in Fig. 5). These results imply that the degree-one structure is found in the models with a wide range for the Rayleigh number, as also shown in mantle convection simulations (McNamara and Zhong, 2005; Yoshida and Kageyama, 2006).

This degree-one convection pattern is similar to the familiar "sluggish-lid regime" or the "transitional regime" in thermal convection of the mantle that has already been found in numerical simulations of mantle convection (e.g., Solomatov, 1995) (Fig. 6b). In this regime, the flow velocities of downwelling plumes from the sluggish-lid are large compared with the interior of the inner core, and the global flow pattern in the sphere corresponds to the temperature distribution. This is because temporal changes in thermal heterogeneity roughly correlate with those in mechanical heterogeneity, as shown in Figs. 3, 4 and 5. Also, once the degree-one structure is formed, the sluggish-lid regime generates the largest magnitude of flow velocity and the most laterally heterogeneous velocity field in the inner convecting region (Figs. 6b and 7a) when compared with other regimes such as the mobile-lid regime (Fig. 6a) and the stagnant-lid regime (Fig. 7b).

SED
7, 3817–3841, 2015

cc BY

When $\Delta\eta_T$ is 10^4 or larger, the scales of the thermal and mechanical heterogeneities under the stagnant-lid, whose thickness is approximately 100 km, are quite small (the dominant degrees are below 16) even after 4.5 Gyr (Fig. 3i–l). Although the relatively long-wavelength mode is intermittently dominant during the simulation even when $\Delta\eta_T$ is quite large ("C" in Fig. 3k–l), it is immediately damped over a short time-scale of ≤ c. 0.5 Gyr. As a result, the stagnant-lid regime is maintained for almost the entire simulation time.

4 Conclusions and discussion

The systematic numerical simulations conducted in this study investigated the possibility of the formation of a degree-one structure with lateral viscosity variations in thermal convection within the age of Earth for a simulated inner core confined in a sphere. The degree-one thermal/mechanical structure, however, only appeared for a limited range of parameter values for lateral viscosity variations. Considering the uncertainties in the exact magnitude of lateral temperature variations, the rheology, and the composition of Earth's inner core materials, the formation of a degree-one structure with lateral viscosity heterogeneity under the limited geophysical conditions confirmed here would be considered possible but not probable for the real Earth. Namely, the degree-one structure of the inner core may have been realized by an "exogenous factor" from outside the ICB, rather than by an "endogenic factor" due to the internal rheological heterogeneity.

An exogenous origin for the hemispherically asymmetric structure of the inner core and the related hemispherical difference in the degree of crystallization, i.e., freezing and melting, of the inner core materials is consistent with a previous suggestion that planetary-scale thermal coupling among the lower mantle, the outer core, and the inner core plays a primary role in the growth and evolution of the inner core (Aubert et al., 2008; Gubbins et al., 2011; Tkalčić, 2015). More recently, a new isotopic geochemical analysis study (Iwamori and Nakamura, 2015; Iwamori et al., 2015) revealed that such planetary-scale thermal coupling operates in the whole-Earth system through

SED
7, 3817–3841, 2015

so-called “top-down hemispheric dynamics”, in which the hemispheric supercontinent-ocean distribution at Earth's surface controls the thermal convection system in the whole Earth via the mantle, outer core, and inner core over the course of Earth's history (see Fig. 13 of Iwamori and Nakamura, 2015).

It should be noted that the style of convection envisioned in this study is only one form of degree-one convection. Another form involves melting and solidification processes at the ICB, as suggested by Alboussière et al. (2010) and Monnereau et al. (2010), who concluded that the inner core translates laterally as a rigid body and the return flow effectively occurs in the fluid outer core. Because the present study adopts impermeable boundary conditions at the ICB, this second form of degree-one convection is not permitted. This scenario provides a strong alternate candidate for the form of degree-one convection through top-down hemispheric dynamics, if degree-one convection due to internal rheological heterogeneity is not possible.

The age of the inner core is one of the most controversial issues in Earth Science. As mentioned in Sect. 2, the value of the total heat flow at the CMB is a key parameter that controls the speed of growth of the inner core. A previous study (Cottaar and Buffett, 2012) has shown that the minimum heat flow for inner core convection is 4.1 TW, giving a maximum inner core age of 1.93 Ga. Heat flow greater than 6.3 TW leads to the present convection regime, but the inner core age is then less than 1.26 Ga. Following their analysis, if the total CMB heat flow is c. 10 TW (Lay et al., 2008 and references therein), the age of inner core should be younger (i.e., less than 1 Ga). If the value of the total CMB heat flow is significantly larger than that used in this study, the possibility of the formation of degree-one structure by an endogenic factor due to rheological heterogeneity becomes less likely, because it takes c. 3.0 Gyr to form the degree-one structure when $\eta_0 = 10^{17}$ Pa s, $k_0 = 36\,\mathrm{W\,m^{-1}\,K^{-1}}$, and $\Delta\eta_T$ is 3.5 (Fig. 3g). At the very least, the conclusion that the convective motion in the inner core is maintained even for the present Earth can be drawn from the models studied here.

Seismic observations provide evidence for a seismic velocity discontinuity about 200 km below the ICB separating an isotropic layer in the uppermost inner core from an underlying anisotropic inner core (e.g., Song and Helmberger, 1998). The results presented here may imply that this "inner core transition zone" represents the boundary between a sluggish, highly viscous, cold layer and an underlying hot convection region (Figs. 6b and 7a). Sumita and Yoshida (2003) predicted that there may be a characteristic structure in the topmost section of the inner core that is similar to the plate tectonic mechanism at Earth's surface, which is explained by the existence of a crust-like, thin, low-degree partial-melting layer and an underlying asthenosphere-like, high-degree partial-melting layer. The ICB is, by definition, at melting temperature, which means that it is possible that the viscosity could be lowest at the top and gradually increase with depth into the interior of the inner core. However, because the temperature across the inner core is never very far from the melting temperature (Stacey and Davis, 2008), depending in detail on the contribution from light element impurities, viscosity variations in the underlying hot convection region should be small.

In future, the evolution of the inner core should be resolved by numerical simulations of the whole-Earth thermal convection system because it is highly possible that the growth rate of the inner core is determined by heat flow at the CMB, which largely depends on the behavior and style of mantle convection (Buffett et al., 1992; Sumita and Yoshida, 2003). The combined effects of the thermal and compositional buoyancies (Lythgoe et al., 2015) and the effects of non-uniform heat flux boundary condition at the ICB, rather than a fixed temperature condition on the style and regime of inner core convection, should also be studied numerically in future.

Acknowledgements. Some figures were produced using the Generic Mapping Tools (Wessel et al., 2013). The calculations presented herein were performed using the supercomputer facilities (SGI ICE-X) at JAMSTEC. The present study was supported by a Grant-in-Aid for Exploratory Research from the Japan Society for the Promotion of Science (JSPS KAKENHI Grant Number 26610144). All of the simulation data are available from the corresponding author upon request.

CC BY

References

Alboussière, T., Deguen, R., and Melzani, M.: Melting-induced stratification above the Earth's inner core due to convective translation, Nature, 466, 744–747, doi:10.1038/nature09257, 2010.
Aubert, J., Amit, H., Hulot, G., and Olson, P.: Thermochemical flows couple the Earth's inner core growth to mantle heterogeneity, Nature, 454, 758–762, doi:10.1038/nature07109, 2008.
Buffett, B.: Earth's core and the geodynamo, Science, 288, 5473, doi:10.1126/science.288.5473.2007, 2000.
Buffett, B. A., Huppert, H. E., Lister, J. R., and Woods, A. W.: Analytical model for solidification of the Earth's core, Nature, 356, 329–331, doi:10.1038/356329a0, 1992.
Cao, A. and Romanowicz, B.: Hemispherical transition of seismic attenuation at the top of the earth's inner core, Earth Planet. Sc. Lett., 228, 243–253, doi:10.1016/j.epsl.2004.09.032, 2004.
Cottaar, S. and Buffett, B.: Convection in the Earth's inner core, Phys. Earth Planet. In., 198, 67–78, doi:10.1016/j.pepi.2012.03.008, 2012.
Creager, K. C.: Large-scale variations in inner core anisotropy, J. Geophys. Res., 104, 23127–23139, doi:10.1029/1999JB900162, 1999.
Davies, G. F.: Ocean bathymetry and mantle convection: 1. Large-scale flow and hot spots, J. Geophys. Res., 93, 10467–10480, doi:10.1029/JB093iB09p10467, 1988.
Davies, G. F. and Richards, M. A.: Mantle convection, J. Geol., 100, 151–206, 1992.
de Koker, N., Steinle-Neumann, G., and Vlček, V.: Electrical resistivity and thermal conductivity of liquid Fe alloys at high P and T, and heat flux in Earth's core, P. Natl. Acad. Sci. USA, 109, 4070–4073, doi:10.1073/pnas.1111841109, 2012.
Deguen, R.: Thermal convection in a spherical shell with melting/freezing at either or both of its boundaries, J. Earth Sci., 24, 669–682, doi:10.1007/s12583-013-0364-8, 2013.
Deguen, R. and Cardin, P.: Thermochemical convection in Earth's inner core, Geophys. J. Int., 187, 1101–1118, doi:10.1111/j.1365-246X.2011.05222.x, 2011.
Deguen, R., Alboussière, T., and Cardin, P.: Thermal convection in Earth's inner core with phase change at its boundary, Geophys. J. Int., 194, 1310–1334, doi:10.1093/gji/ggt202, 2013.
Deuss, A., Irving, J. C. E., and Woodhouse, J. H.: Regional variation of inner core anisotropy from seismic normal mode observations, Science, 328, 1018–1020, doi:10.1126/science.1188596, 2010.

SED
7, 3817–3841, 2015

A simple 3-D numerical model of thermal convection in Earth's growing inner core

M. Yoshida

Title Page
Abstract Introduction
Conclusions References
Tables Figures
◀◀ ▶▶
◀ ▶
Back Close
Full Screen / Esc
Printer-friendly Version
Interactive Discussion

CC BY

Dziewonski, A. M. and Anderson, D. L.: Preliminary reference earth model, Phys. Earth Planet. In., 25, 297–356, doi:10.1016/0031-9201(81)90046-7, 1981.
Gubbins, D., Sreenivasan, B., Mound, J., and Rost, S.: Melting of the Earth's inner core, Nature, 473, 361–363, doi:10.1038/nature10068, 2011.
Irving, J. C. E. and Deuss, A.: Stratified anisotropic structure at the top of Earth's inner core: a normal mode study, Phys. Earth Planet. In., 186, 59–69, doi:10.1016/j.pepi.2011.03.003, 2011.
Iwamori, H. and Nakamura, H.: Isotopic heterogeneity of oceanic, arc and continental basalts and its implications for mantle dynamics, Gondwana. Res., 27, 1131–1152, doi:10.1016/j.gr.2014.09.003, 2015.
Iwamori, H., Nakamura, H., and Yoshida, M.: East–west mantle geochemical hemispheres and its implications for a coupled supercontinent-mantle-core dynamics, Proc. 26 General Assembly of IUGG, IUGG-2295, Prague, Czech Republic, IUGG-2295, 2015.
Jacobs, J. A.: The Earth's inner core, Nature, 172, 297–298, doi:10.1038/172297a0, 1953.
Karato, S.: The dynamic structure of the deep Earth, in: An Interdisciplinary Approach, Princeton Univ. Press, Princeton, USA, 241 pp., 2003.
Karato, S. and Wu, P.: Rheology of the upper mantle: a synthesis, Science, 260, 771–778, doi:10.1126/science.260.5109.771, 1993.
Lay, T., Hernlund, J., and Buffett, B. A.: Core-mantle heat flow, Nat. Geosci., 1, 25–32, doi:10.1038/ngeo.2007.44, 2008.
Lister, J. R. and Buffett, B. A.: Stratification of the outer core at the core-mantle boundary, Phys. Earth Planet. In., 105, 5–19, doi:10.1016/S0031-9201(97)00082-4, 1998.
Lythgoe, K. H., Deuss, A., Rudge, J. F., and Neufeld, J. A.: Earth's inner core: innermost inner core or hemispherical variations?, Earth Planet. Sc. Lett., 385, 181–189, doi:10.1016/j.epsl.2013.10.049, 2014.
Lythgoe, K. H., Rudge, J. F., Neufeld, J. A., and Deuss, A.: The feasibility of thermal and compositional convection in Earth's inner core, Geophys. J. Int., 201, 764–782, doi:10.1093/gji/ggv034, 2015.
McNamara, A. K. and Zhong, S.: Degree-one mantle convection: dependence on internal heating and temperature-dependent rheology, Geophys. Res. Lett., 32, L01301, doi:10.1029/2004GL021082, 2005.
Monnereau, M., Calvet, M., Margerin, L., and Souriau, A.: Lopsided growth of Earth's inner core, Science, 328, 1014–1017, doi:10.1126/science.1186212, 2010.

CC BY

Niu, F. and Wen, L.: Hemispherical variations in seismic velocity at the top of the Earth's inner core, Nature, 410, 1081–1084, doi:10.1038/35074073, 2001.
Pozzo, M., Davies, C., Gubbins, D., and Alfè, D.: Thermal and electrical conductivity of iron at Earth's core conditions, Nature, 485, 355–358, doi:10.1038/nature11031, 2012.
Pozzo, M., Davies, C., Gubbins, D., and Alfè, D.: Thermal and electrical conductivity of solid iron and iron-silicon mixtures at Earth's core conditions, Earth Planet. Sc. Lett., 393, 159–164, doi:10.1016/j.epsl.2014.02.047, 2014.
Schubert, G., Turcotte, D. L., and Olson, P.: Mantle Convection in the Earth and Planets, Cambridge Univ. Press, UK, 2001.
Sleep, N. H.: Hotspots and mantle plumes: some phenomenology, J. Geophys. Res., 95, 6715–6736, doi:10.1029/JB095iB05p06715, 1990.
Solomatov, V. S.: Scaling of temperature- and stress-dependent viscosity convection, Phys. Fluids., 7, 266–274, doi:10.1063/1.868624, 1995.
Song, X. and Helmberger, D. V.: Seismic evidence for an inner core transition zone, Science, 282, 924–927, doi:10.1126/science.282.5390.924, 1998.
Stacey, F. D. and Davis, P. M.: Physics of the Earth, 4th edn., Cambridge Univ. Press, UK, 532 pp., 2008.
Stevenson, D. J.: Models of the Earth's core, Science, 214, 611–619, doi:10.1126/science.214.4521.611, 1981.
Sumita, I. and Yoshida, S.: Thermal interactions between the mantle, outer and inner cores, and the resulting structural evolution of the core, in: Earth's Core: Dynamics, Structure, Rotation, edited by: Dehant, V., Creager, K. C., Karato, S., and Zatman, S. Am. Geophys. Un., New York, USA, 213–231, 2003.
Tanaka, S. and Hamaguchi, H.: Degree one heterogeneity and hemispherical variation of anisotropy in the inner core from *PKP*(BC)–*PKP*(DF) times, J. Geophys. Res., 102, 2925–2938, doi:10.1029/96JB03187, 1997.
Tkalčić, H.: Complex inner core of the Earth: the last frontier of global seismology, Rev. Geophys., 53, 59–64, doi:10.1002/2014RG000469, 2015.
Turcotte, D. L. and Schubert, G.: Geodynamics, 3rd edn., Cambridge Univ. Press, UK, 2014.
Verhoogen, J.: Energetics of the Earth, National Academies Press, Washington, DC, USA, 139 pp., 1980.

Vočadlo, L., Alfè, D., Gillan, M. J., and Price, G. D.: The properties of iron under core conditions from first principles calculations, Phys. Earth Planet. In., 140, 105–125, doi:10.1016/j.pepi.2003.08.001, 2003.

Waszek, L., Irving, J., and Deuss, A.: Reconciling the hemispherical structure of Earth's inner core with its super-rotation, Nat. Geosci., 4, 264–267, doi:10.1038/ngeo1083, 2011.

Wessel, P., Smith, W. H. F., Scharroo, R., Luis, J. F., and Wobbe, F.: Generic Mapping Tools: improved version released, EOS Trans. AGU, 94, 409–410, doi:10.1002/2013EO450001, 2013.

Yoshida, M.: Mantle convection with longest-wavelength thermal heterogeneity in a 3-D spherical model: degree one or two?, Geophys. Res. Lett., 35, L23302, doi:10.1029/2008GL036059, 2008.

Yoshida, M.: Effects of various lithospheric yield stresses and different mantle-heating modes on the breakup of the Pangea supercontinent, Geophys. Res. Lett., 41, 3060–3067, doi:10.1002/2014GL060023, 2014.

Yoshida, M. and Kageyama, A.: Application of the Yin-Yang grid to a thermal convection of a Boussinesq fluid with infinite Prandtl number in a three-dimensional spherical shell, Geophys. Res. Lett., 31, L12609, doi:10.1029/2004GL019970, 2004.

Yoshida, M. and Kageyama, A.: Low-degree mantle convection with strongly temperature- and depth-dependent viscosity in a three-dimensional spherical shell, J. Geophys. Res., 111, B03412, doi:10.1029/2005JB003905, 2006.

Table 1. Physical parameters for the simulation used in this study.

Symbol	Definition	Value	Unit	Refs.
α_0	Thermal expansion coefficient[1]	9.74×10^{-6}	K^{-1}	a, b
c_{p0}	Specific heat at constant pressure[1]	7.03×10^{2}	$J\,kg^{-1}\,K^{-1}$	a
g_0	Gravitational acceleration[1]	4.4002	$m\,s^{-2}$	a
ρ_0	Density[1]	1.27636×10^{4}	$kg\,m^{-3}$	a
k_0	Thermal conductivity[1]	36 or 200	$W\,m^{-1}\,K^{-1}$	a, c, d, e
κ_0	Thermal diffusivity[1]	4.01×10^{-6}	$m^2\,s^{-1}$	a
η_0	Viscosity[1]	10^{17} or 10^{16}	Pa s	f
–	Temperatures at the inner core boundary and Earth's center	5000 and 5030	K	a
ΔT_0	Temperature difference across the inner core[1]	30	K	a
M_m	Mass of the mantle	4.043×10^{24}	kg	g
τ_c	Formation age of the core	4.5	Ga	h
c_{pe0}	Average specific heat at constant pressure for Earth	9.2×10^{2}	$J\,kg^{-1}\,K^{-1}$	g
ρ_{e0}	Average density of Earth	5.520×10^{3}	$kg\,m^{-3}$	g
T_m	Mean mantle temperature	2250	K	g
E_a	Activation energy for dry olivine	540×10^{3}	$J\,mol^{-1}$	g, i
λ	Average decay constant for the mixture of radioactive isotopes in the mantle	2.77×10^{-10}	yr^{-1}	g
$dT/dt\|_{t=t_0}$	Present cooling rate of the mantle	64.7	$K\,Gyr^{-1}$	Eq. (7)
G	Gravitational constant	6.67384×10^{-11}	$m^3\,kg^{-1}\,s^{-2}$	g
R	Gas constant	8.3144621	$J\,mol^{-1}\,K^{-1}$	g
$\partial T_s/\partial p$	Solidification profile	7×10^{-9}	$K\,Pa^{-1}$	j, k
r_e	Radius of Earth	6.371×10^{6}	m	g
r_b	Radius of the outer core	3.48×10^{6}	m	l
$r_c(t)$	Radius of the inner core	Time-dep.	m	–
r_c	Radius of the present inner core	1.2215×10^{6}	m	l
r_c^i	Initial radius of the inner core	2.15×10^{4}	m	2
Ω	Model constant (see text)	1.13×10^{13}	W	Eq. (6)
N	Model constant (see text)	2.01×10^{16}	$J\,m^{-2}$	Eq. (11)
F'_m	Model constant (see text)	2.56×10^{12}	W	Eq. (12)
Dimensionless parameters				
$Ra(t)$	Thermal Rayleigh number	Time-dep.	–	Eq. (5)
$H(t)$	Internal heat-source number	Time-dep.	–	Eq. (5)
$\zeta(t)$	Spherical-shell ratio number	Time-dep.	–	Eq. (5)

Definition: [1] indicates reference values for the inner core. References: [a] Stacey and Davis (2008); [b] Vočadlo et al. (2003); [c] de Koker et al. (2012); [d] Pozzo et al. (2012); [e] Pozzo et al. (2014); [f] Karato (2003); [g] Turcotte and Schubert (2014); [h] Lister and Buffett (1998); [i] Karato and Wu (1993); [j] Verhoogen (1980); [k] Buffett et al. (1992); [l] Dziewonski and Anderson (1981). [2] indicates arbitrary values (see text).

CC BY

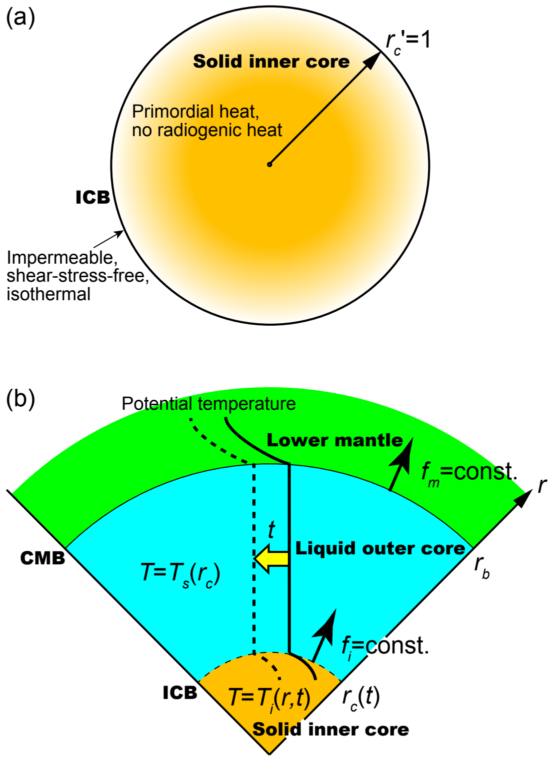

Figure 1. (a) Illustration for the numerical model of inner core convection. **(b)** Schematic profile of the potential temperature in the cooling core of the Earth used in an analytical model for solidification of the inner core (after Buffett et al., 1992). The solid line represents the temperature in the upper part of the thick solid inner core, the liquid outer core, and the lower mantle at some instant. The thick dashed line represents the subsequent evolution of temperature as heat is continuously extracted from the core. Heat fluxes f_m and f_i pertain to the core-mantle and inner-core boundaries (CMB and ICB), respectively. The solidification temperature $T_s(r_c)$ is defined at the ICB, and $T_s(r, t)$ is the temperature within the inner core.

SED
7, 3817–3841, 2015

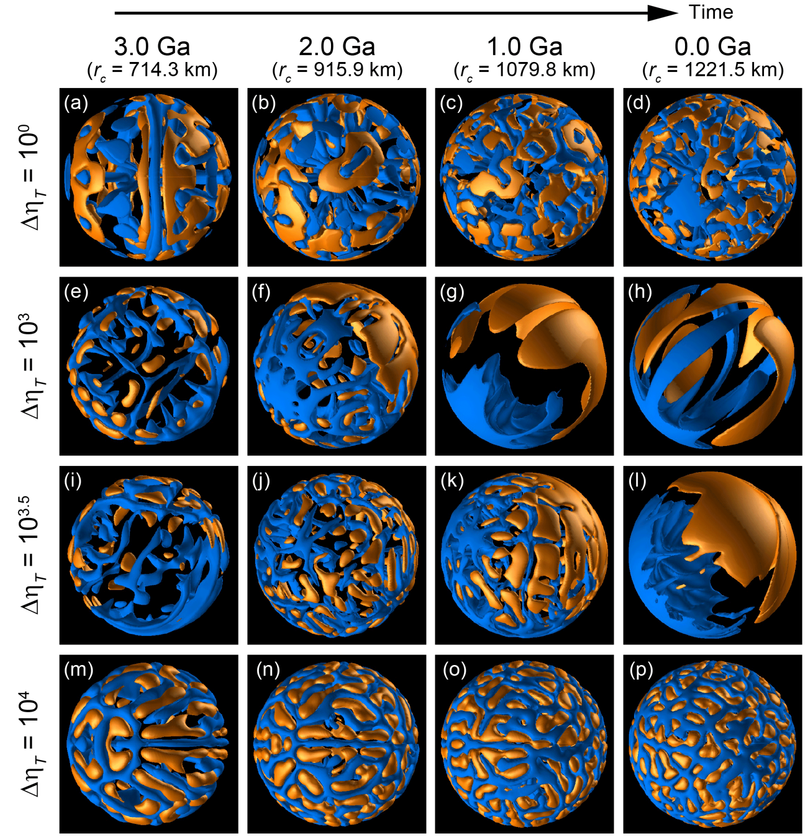

Figure 2. Time evolution of the convection pattern in the inner core for models with $\eta_0 = 10^{17}$ Pa s, $k_0 = 36\,\mathrm{W\,m^{-1}\,K^{-1}}$, and **(a–d)** $\Delta\eta_T = 10^0$, **(e–h)** $\Delta\eta_T = 10^3$, **(i–l)** $\Delta\eta_T = 10^{3.5}$, and **(m–p)** $\Delta\eta_T = 10^4$. Blue and copper isosurfaces indicate regions with lower and higher than average temperatures at each depth. (**a–d** and **m–p**) blue: −0.3 K; copper: +0.3 K. (**e–f** and **i–k**) blue: −0.6 K; copper: +0.6 K. (**g**, **h** and **l**) blue: −1.5 K; copper: +1.5 K.

SED
7, 3817–3841, 2015

A simple 3-D numerical model of thermal convection in Earth's growing inner core

M. Yoshida

CC BY

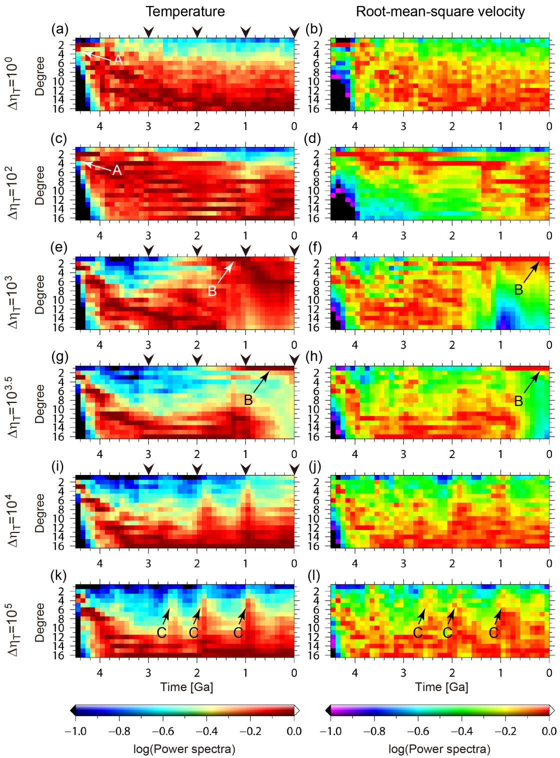

Figure 3. Temporal changes in the heterogeneity of temperature and root-mean-square velocity fields in the inner core for the models with $\eta_0 = 10^{17}$ Pa s, $k_0 = 36\,\mathrm{W\,m^{-1}\,K^{-1}}$, and **(a–b)** $\Delta\eta_T = 10^0$, **(c–d)** $\Delta\eta_T = 10^2$, **(e–f)** $\Delta\eta_T = 10^3$, **(g–h)** $\Delta\eta_T = 10^{3.5}$, **(i–j)**, $\Delta\eta_T = 10^4$, and **(k–l)** $\Delta\eta_T = 10^5$. The logarithmic power spectra are normalized by the maximum values at each elapsed time. The four black wedges on the panels **(a)**, **(e)**, **(g)**, and **(i)** represent the ages that correspond to Fig. 2.

CC BY

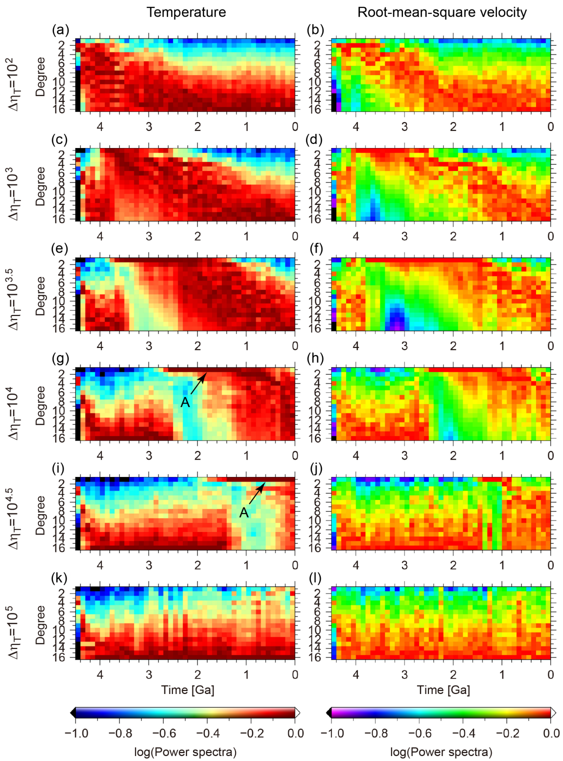

Figure 4. Temporal changes in the heterogeneity of temperature and root-mean-square velocity fields in the inner core for the models with $\eta_0 = 10^{16}$ Pa s, $k_0 = 36\,\mathrm{W\,m^{-1}\,K^{-1}}$, and **(a–b)** $\Delta\eta_T = 10^0$, **(c–d)** $\Delta\eta_T = 10^2$, **(e–f)** $\Delta\eta_T = 10^3$, **(g–h)** $\Delta\eta_T = 10^{3.5}$, **(i–j)**, $\Delta\eta_T = 10^4$, and **(k–l)** $\Delta\eta_T = 10^5$. The logarithmic power spectra are normalized by the maximum values at each elapsed time.

SED
7, 3817–3841, 2015

A simple 3-D numerical model of thermal convection in Earth's growing inner core

M. Yoshida

CC BY

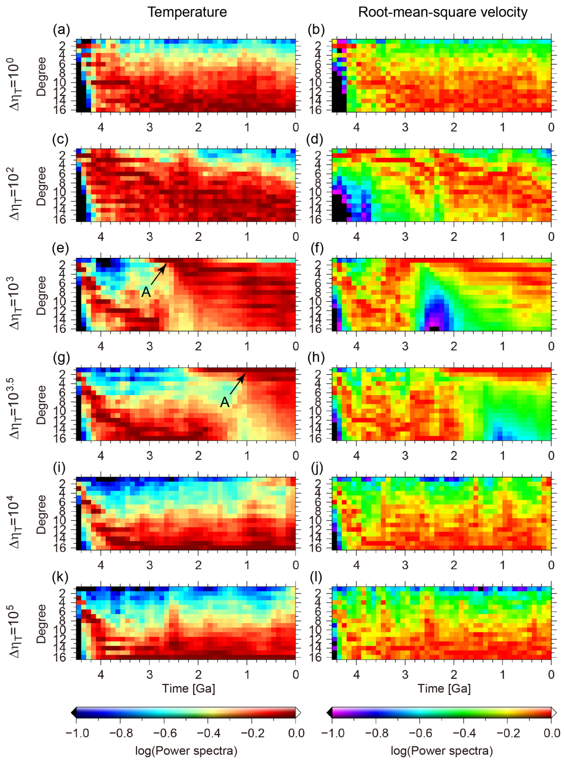

Figure 5. Temporal changes in the heterogeneity of temperature and root-mean-square velocity fields in the inner core for the models with $\eta_0 = 10^{16}$ Pa s, $k_0 = 200$ W m^{-1} K^{-1}, and **(a–b)** $\Delta\eta_T = 10^0$, **(c–d)** $\Delta\eta_T = 10^2$, **(e–f)** $\Delta\eta_T = 10^3$, **(g–h)** $\Delta\eta_T = 10^{3.5}$, **(i–j)**, $\Delta\eta_T = 10^4$, and **(k–l)** $\Delta\eta_T = 10^5$. The logarithmic power spectra are normalized by the maximum values at each elapsed time.

SED
7, 3817–3841, 2015

CC BY

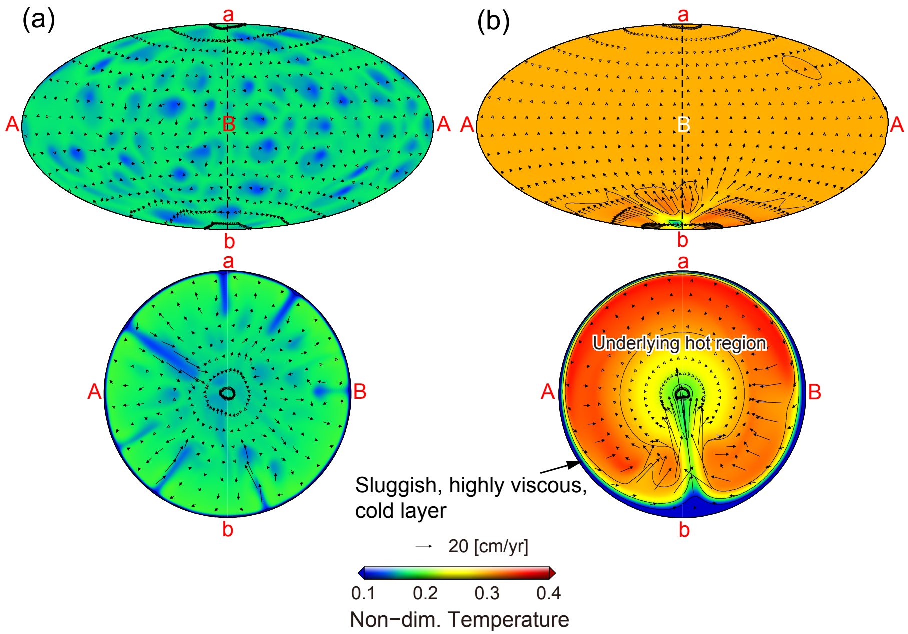

Figure 6. Cross sections of temperature and velocity fields for the models with $\eta_0 = 10^{17}$ Pa s, $k_0 = 36\,\mathrm{W\,m^{-1}\,K^{-1}}$, and **(a)** $\Delta\eta_T = 10^0$ and **(b)** $\Delta\eta_T = 10^3$ at 0.0 Ga. The top panels show the cross sections at the central depth of the inner core (i.e., radius of 610.8 km) and bottom panels show the cross sections cut along the great circles shown by dashed lines in the top panels. The contour interval in the temperature plots is 3 K. These figures correspond to **(a)** Figs. 2d and 3a, and **(b)** Figs. 2h and 3e.

SED
7, 3817–3841, 2015

A simple 3-D numerical model of thermal convection in Earth's growing inner core

M. Yoshida

CC BY

SED
7, 3817–3841, 2015

A simple 3-D numerical model of thermal convection in Earth's growing inner core

M. Yoshida

CC BY

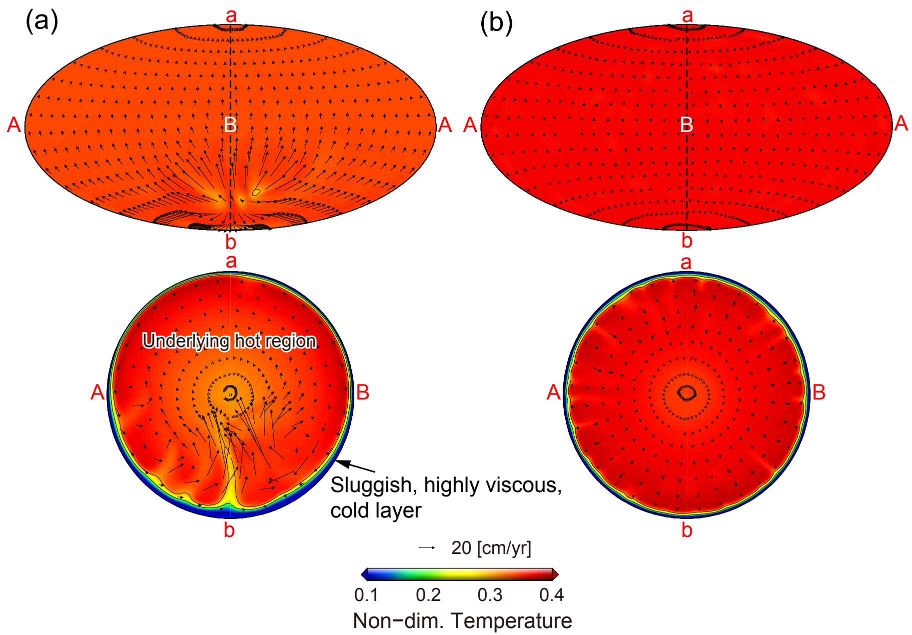

Figure 7. Cross sections of temperature and velocity fields for the models with $\eta_0 = 10^{17}$ Pa s, $k_0 = 36\,\mathrm{W\,m^{-1}\,K^{-1}}$, and **(a)** $\Delta\eta_T = 10^{3.5}$ and **(b)** $\Delta\eta_T = 10^4$ at 0.0 Ga. The top panels show the cross sections at the central depth of the inner core (i.e., radius of 610.8 km) and bottom panels show the cross sections cut along the great circles shown by dashed lines in the top panels. The contour interval in the temperature plots is 3 K. These figures correspond to **(a)** Figs. 2l and 3g, and **(b)** Figs. 2p and 3k.